Chapter 8

Impact of the Glancing Angle Deposition on the Yttria-Stabilized Zirconia Growth and Their Thermal Barrier Coating Properties

Cesar Amaya, John Jairo Prıas-Barragan,
Julio Cesar Caicedo, Jose Martin Yañez-Limon and
Gustavo Zambrano

Additional information is available at the end of the chapter

http://dx.doi.org/10.5772/intechopen.81905

Abstract

Yttria-stabilized zirconia (YSZ) is the most common material used as a thermal barrier in several engineering applications. The majority of films produced by physical vapor deposition (PVD) techniques use normal incidence and lead to the columnar growth normal to the substrate. The typical columnar structure of sputter-deposited films is largely influenced, among other parameters, by pressure, temperature, thickness, and the ion-to-atom ratio incident at the substrate or substrate bias voltage. Another important experimental parameter used to modify the film properties is the direction of the incident flux of the depositing species with respect to the substrate surface. In this chapter an oblique angle deposition (OAD) approach was used to grow YSZ with tilted columnar structures, to study the impact of this deposition technique on the microstructure, morphology, and, correspondingly, the thermal conductivity of YSZ films, in order to improve the insulator potential of these thin films. Additionally, in the chapter, we present a detailed description of the oblique angle deposition (OAD) technique and double-layer model used for determination of the effective thermal conductivity of YSZ samples grown over thick substrates.

Keywords: physical vapor deposition, yttria-stabilized zirconia (YSZ), oblique angle deposition (OAD), thermal conductivity, double-layer model

1. Introduction

Yttria-stabilized zirconia (YSZ) coating systems are widely used for the thermal, oxidation, and hot corrosion protection of high-temperature components in gas turbine and diesel engines [1], and, additionally, the electrolyte YSZ is the standard ionic conductor [2] used in fuel cells, being a brittle material due to its high hardness [3]. This thermal and oxidation protection must be achieved without incurring excessive thermomechanical loading of the coating system and the metal component to which it is applied.

For the thermal, oxidation, and hot corrosion protection of high-temperature components, the multifunctional requirements of these coatings dictate the use of a coating system consisting of three separate layers: a porous, 7–8 wt.% yttria-stabilized zirconia (7–8YSZ) thermal barrier coating (TBC) which provides thermal insulation, a thermally grown (α-alumina) oxide (TGO) layer which inhibits oxygen transport to the component, and a low-sulfur platinum aluminide or MCrAlY (where M is Ni or Co) bond coat [4, 5]. Usually, the TBC thick layer (the thickness is typically of hundreds of microns) is deposited either by air plasma spray (APS) [6] or electron beam physical vapor deposition (EB-PVD) [7]. Low-pressure plasma spray (LPPS) [5] or pack cementation [8] is used to apply the bond coat. Oxidation of the bond coat prior to or during deposition of the TBC layer (and later during service) forms the ($\sim$1 mm) TGO layer. However, for other applications the YSZ TBC thin films can be deposited by sputtering and pulsed laser deposition (PLD). In both cases, the typical columnar structure of sputter or pulsed laser deposited films is largely influenced, among other parameters, by pressure, temperature, thickness, and the ion-to-atom ratio incident at the substrate or substrate bias voltage [9–11]. This morphology is expected to follow the structure zone model of Thornton [12] and could be overcome by an increase of the deposition temperature.

YSZ is the currently preferred TBC layer material for gas turbine engine applications because of its low thermal conductivity, k, its relatively high (compared to other ceramics) thermal expansion coefficient, and its good erosion resistance [13]. The low thermal conductivity of bulk YSZ is a result of the low intrinsic thermal conductivity of zirconia and the addition of yttria [14]. An yttria concentration in the range of 6–8 wt.% is generally used since this composition maximizes spallation life due to the formation of the metastable t′ phase [13]. This phase yields a complex microstructure which resist crack propagation and transformation into the monoclinic phase (4% volume change) upon cooling. The result is a thermomechanically tough TBC layer with a room temperature, grain size dependent, and thermal conductivity of 2.2–2.6 W/m K in the densest (bulk) form [15]. The thermal protection and spallation lifetimes of YSZ TBC layers produced via different deposition techniques differ significantly. TBC coatings produced by APS have a thermal conductivity in the range of 0.8–1.0 W/m K at 25°C [1, 14, 16]. This is significantly lower than the 1.5–1.9 W/m K reported for EB-PVD coatings at 25°C [1, 17]. On the other hand, for YSZ thin films obtained by different techniques, the thermal conductivity values depend on the grain size, and these are in the range between 0.6 and 1.8 W/m K for grain sizes between 10 and 100 nm [18, 19].

Usually, there are two ways to reduce the thermal conductivity of YSZ TBC obtained by physical vapor deposition (PVD). The first one is the addition of dopants, in this case the

http://dx.doi.org/10.5772/intechopen.81905

addition of rare earth oxides (REO). Klemens et al. [20] conclude that co-doping with REO can solve the problems concerning the high-temperature (tetragonal) phase stability of ZrO_2 and important decreases in thermal conductivity can be achieved by approaching values obtained by APS (k = 0.8 W/mK). The second way is to manipulate the microstructure of the coating, which basically involves including fields of stresses and interfaces to the interior of the material, in such a way that they act as centers of dispersion of the phonons. In the study conducted by Soyez et al. [21] on YSZ nanocrystalline, the dependence of the thermal conductivity with the grain size in nanocrystals of YSZ, for films with thicknesses of 0.5 and 1.2 μm and yttria compositions between 8 and 15 mol.%, was observed. Another approach to the effect of the structure variation to micro- and nanoscale is to use multilayers, since the value of the coating thermal resistance in the form of multilayers is the sum in a series of the thermal resistances of the interfaces where the interaction between the phonon and the scattering centers that are in them occurs. For applications at high temperatures, coatings can be designed in nanostructured multilayer sequences. For example, studies have been conducted on multilayer systems of Al_2O_3/YSZ obtained via EB-PVD and multilayer YSZ/SiO_2 [22] obtained via ion beam-PVD, but the thermal conductivity measurements obtained show no significant decreases, regardless of the materials, the technique, and the number of layers used [23]. In addition to the grain size and the generation of interfaces using multilayer systems, the effect of the thickness of the coating on its thermal conductivity must be taken into account. In the model proposed by Nicholls [24], two characteristic zones of the ceramic coatings obtained by the EB-PVD technique are presented: the internal zone of fine grain and the external zone of coarse grain. The thermal conductivity of the internal zone of fine grain is much lower than the thermal conductivity of the external zone, due to a greater density of grain boundaries as well as to numerous oblique columnar limits in the internal zone, since there is a multiple nucleation and subsequent growth of the columnar microstructure. Thus, the thermal conductivity in this area is dominated by the dispersion of phonons with defects and grain boundaries in this part of the coating, resulting in a low thermal conductivity of around 1.0 W/m K at room temperature. In this way, the total thermal conductivity of the coating will be the result of the combined effect of these two zones, so if the total thickness of the coating is equal to the thickness of the internal zone, the total thermal conductivity will be equal to that of this area; therefore, it will be lower. Obtaining this type of TBC microstructure can be achieved using the "shuttering" method, which consists in the periodic interruption of the vapor flow of atoms. Using this technique Wolfe et al. [25] reported a ∼10% decrease in the thermal conductivity of 8YSZ coatings deposited by EB-PVD. Summarized, creating imperfections within the network, the phonons free path could change producing a greater dispersion and decreasing the thermal conductivity.

In the same way, another important experimental parameter used to modify the micro- and nanostructure is to change the direction of the incident flux of the depositing species respecting the substrate surface. Most of films produced by PVD techniques use normal incidence and lead to the columnar growth normal to the substrate. Depositions at oblique angles or sculptured thin films were first reported in 1959 [26] and later by others [27–29] and are often referred to as glancing angle deposition (GLAD). The structure is achieved when the substrate is tilted and forms a high angle between the material flux and substrate surface. In this way, in the microstructure, the column growth direction follows the orientation of the material flux,

typically performed by directional deposition techniques, such as PVD. Several studies have been conducted to elucidate the influence of the thin-film microstructure grown by PVD under GLAD technique on the morphology and structure [30, 31] of different thin-film materials, as well as on their mechanical, [3] electrical [31], and optical properties [33, 34]. On the other hand, previously Hass et al. [35] conducted a study with a TBC layer deposited by electron beam evaporation technique (EB-PVD), but placing the substrate inclined with respect to the vapor flux, to obtain a zigzag-shaped pore microstructure that greatly reduced the thermal conductivity.

In this chapter we present the sculpturing of YSZ thin films using radio-frequency (r.f.) magnetron sputtering under oblique incidence with respect to the normal substrate surface.

2. Glancing angle deposition technique

In the last decades, the physical deposition in vapor phase (PVD) of films and coatings at different incident angles of the steam flow has arisen as an alternative for the control of the morphology, distribution, and shape of the pores present throughout the thickness of the coating as a result of a "shading" effect which is influenced by the angle of incidence of the atoms arriving on the substrate. All this leads to a challenge from the technological point of view focused on obtaining an oblique angle deposit in situ, with sufficient versatility and reproducibility that allows obtaining coatings with "customized" microstructures for various applications. This approach is commonly referred to as glancing angle deposition (GLAD) or oblique angle deposition (OAD), which in this case results in YSZ coatings with an inclined columnar microstructure. In order to obtain this microstructure, the substrate is inclined at an angle (α) with respect to the vapor incident flow on the substrate plane, as it can be seen schematically in **Figure 1**.

When the coatings are deposited on substrates of low roughness, the films obtained by OAD consist of randomly distributed columns with strong competition between the growing

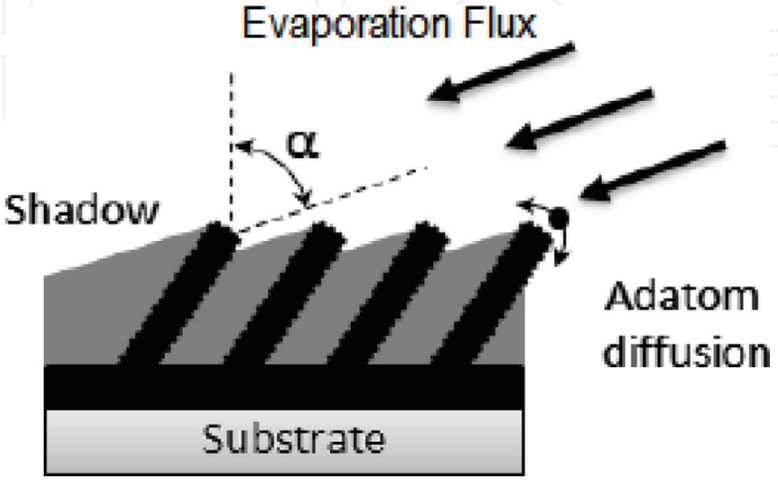

Figure 1. Geometry of oblique angle deposition.

http://dx.doi.org/10.5772/intechopen.81905

columns, where some grow at the expense of the adjacent ones. The randomness of the columns results in inhomogeneous properties of the film in the plane parallel to the substrate, while the competition between the growing columns makes the films nonuniform in the direction along the normal to the substrate. Since the shading effect is the main mechanism, the higher values of α lead to a more pronounced porosity. This occurs because the shading effect generates areas where the vapor flow cannot directly reach the nuclei of atoms on the surface and, therefore, the shadow effect is widely favored [36] leading to a porous columnar microstructure of isolated grains and inclined toward the vapor source. Therefore, the columns do not grow parallel to the direction of the incident vapor flow, and the microstructure tilt can be generated by changing the substrate inclination angle. **Figure 2** shows a schematic illustration of the growth mechanism of micro-columnar structures.

To achieve a glancing angle deposition, the geometry of a conventional sputtering setup was modified similar to some studies reported by others [31]. For this study, the deposition angle of the substrate was fixed at 45° with respect to the incident flux. Additionally, in-plane rotations of 180° were performed to obtain a "zigzag"-like morphology and stop the deposition when the rotation was completed. **Figure 3(a)** and **(b)** shows the experimental setup used in the present study for the in-plane rotations of 180° to obtain "zigzag"-like growth morphology

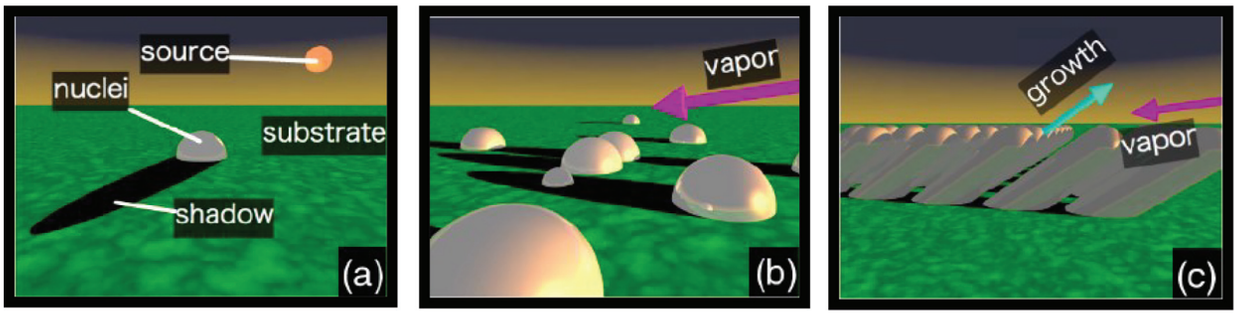

Figure 2. Schematic illustrations of the growth mechanism of micro-columnar structures by OAD: (a) nucleation, (b) onset of self-shadowing, and (c) micro-columnar growth.

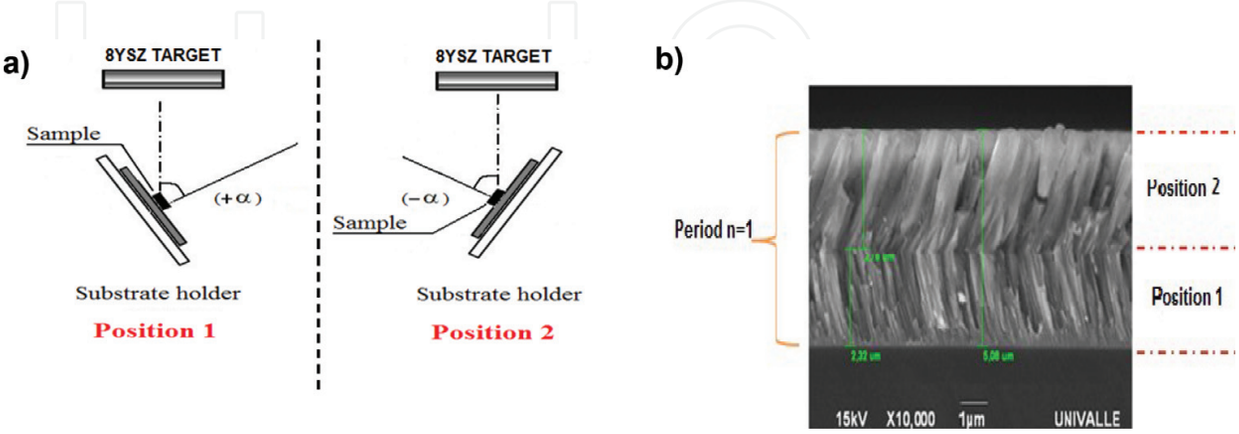

Figure 3. (a) Experimental setup used for the in-plane 180° rotations to obtain "zigzag"-like growth morphology. (b) Scanning electron microscopy (SEM) cross-sectional view of YSZ thin film grown under this configuration at a period of n = 1.

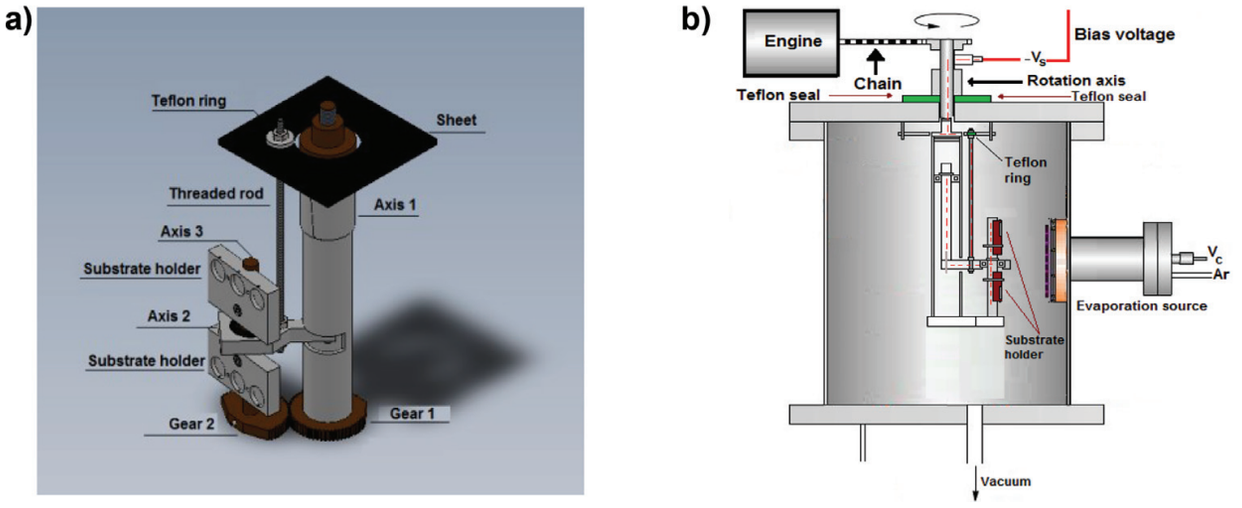

Figure 4. (a) 3D model of the designed device. (b) Illustrative diagram of the device inside the vacuum deposition chamber.

and the SEM cross-sectional view of YSZ thin film grown under this configuration at a period of n = 1, respectively.

However, in practice the substrate rotation must be controlled by a mechanism that allows the transmission of movement inside the vacuum chamber and at the same time be operative for the deposit conditions such as pressure, temperature, bias voltage, etc. To achieve this goal, it was necessary to design a mechanism that would allow to transmit this movement but without modifying the location of the substrate surface with respect to the flow of evaporated material, since if this occurs, the substrate would be in an area that would be outside of the material flow affecting the deposition rate and the shading effect. To solve this problem, a device was designed [37] based on a cylinder with three axes and two bearings that can withstand high temperatures. On the other hand, to provide greater stability during the substrate holder movement, a tie is added consisting of a threaded rod which passes through axis 3 and is coupled to a sheet on the upper part of the device, which is not in contact with axis 1 (see **Figure 4a**). **Figure 4b** illustrates the device inside the vacuum deposition chamber, indicating the arrangement that allows the application of a polarizing voltage to the substrate (bias voltage).

A detailed description of the experimental procedure and deposition parameters used for 8 mol.% YSZ TBC film growth was previously reported by Amaya et al. [19]. To obtain the "zigzag" structure, initially the period *(n)* like the repetition unit composed by two layers was defined, each grown with an angle of +45° and −45°, respectively, and the spatial period (Λ), the bilayer thickness. We systematically varied *n* (1, 2, 10, 30, 50, and 70), keeping the total thickness (3.50 μm) of the multilayer constant. For this reason, the spatial period will be smaller when *n* increases.

3. Thermal conductivity determination

High thermal conductivity materials are widely used in heat dissipation applications, and materials with low thermal conductivity are used as thermal insulators, for example, the YSZ

material studied in this work. In general, the thermal conductivity of a material may depend on the temperature; however, in this work, all measurements of the thermal conductivity in YSZ were made at room temperature.

Among the techniques used for the determination of thermal transport, parameters are the techniques in steady-state and transient or frequency-dependent techniques. In the first case, the thermal conductivity is directly determined, and in the second case, the thermal diffusivity (α) is measured, through which the thermal conductivity (k) can be estimated if the density (ρ) and the specific heat (c_p) of the sample under study are known, by means of the expression $\alpha = k/\rho c_p$.

Within the transient and frequency-dependent techniques are the laser-flash technique [38], thermal lens spectroscopy [39], photoacoustic spectroscopy in its different modalities of open cell [40], closed cell [41], two-beam cell [42], etc.; as well as the photoelectric spectroscopy [43]. These techniques are very appropriate in the case of bulk samples, but they have their instrumental complication and limitations in the case of thin coatings. The techniques of 3w [44] and thermoreflectance [45] are the most used in the determination of the thermal conductivity of coatings and thin films, for which a sophisticated instrumentation is required in the case of thermoreflectance and additionally adequate preparation of the small metallic elements deposited on the material to be studied to heat and temperature monitoring in the case of the 3w technique.

In order to find the thin film's thermal conductivity value, a hot plate technique as an appropriate thermal conductivity measurement system was used [46]. In this technique, it was assumed that the transfer of heat is by conduction through the YSZ film; the thermal conductivity measurement experimental setup is shown in **Figure 5**. The sample is placed on the heater, which increases the temperature to 373 K, where it remains stable, until that the heat reservoir comes into contact with the sample and then the heat is transferred from the heater to the heat reservoir through the sample; this variation is sensed using solid-state sensors.

Considering the heat energy conservation law in the thermal system as presented in **Figure 5**, it is possible to obtain the thermal power differences between heater and heat reservoir as following:

$$P_H - P_R = 0 \tag{1}$$

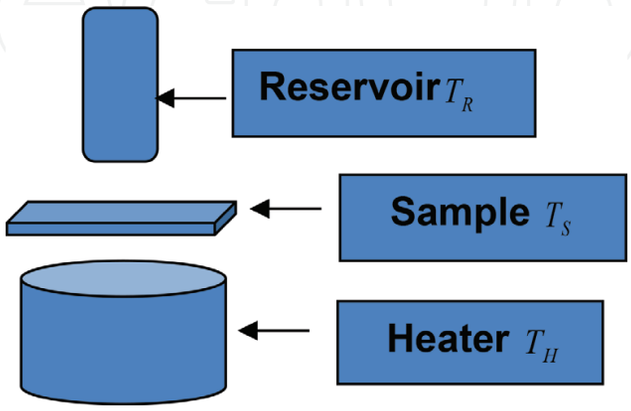

Figure 5. Thermal conductivity measurement experimental setup [46].

where these thermal powers are given by:

$$P_H = \frac{(T_C - T)KA}{l} \quad P_R = cM\frac{dT}{dt} \tag{2}$$

where T_C and T are the heater temperature and the variation of temperature, respectively; K is the thermal conductivity of the material; l and A are the thickness and area of the sample, respectively; and M and c are the mass and the specific heat of the heat reservoir, respectively.

Equating these thermal powers and solving the first-order differential expression, the temperature evolution of the process can be described, given by

$$\Delta T_R = T_H e^{-t/\tau} + T_S \tag{3}$$

where ΔT_R, T_H, and T_S are the temperature variation in the heat reservoir, the temperature in the heater, and the temperature in the sample, respectively, and t and τ are the time and the inverse of the slope, which is directly related to the thermal conductivity of the sample. Therefore, the thermal conductivity of the material can be calculated as

$$K = \frac{lcM}{\tau A} \tag{4}$$

The effective thermal conductivity in the samples as film growth over substrates can be obtained by using the double-layer method [47, 48]. In this method, the total thermal resistance is the sum of the film and substrate thermal resistances, and knowing the sample geometry and thermal conductivity of the substrate, it is possible to calculate the effective value of the thermal conductivity in the film as was proposed by Mansanares et al. [47, 48].

The thermal conductivity of YSZ over glass substrates can be determined by considering the double-layer model as follows.

Figure 6 shows a schematic representation of the total thermal resistance by the superposition of thermal resistances between YSZ film and glass substrate. This representation can be written as the sum of thermal resistances [46–48]:

$$R_T = R_{YSZ} + R_{Glass} \tag{5}$$

Here, R_T, R_{YSZ}, and R_{Glass} are the total, YSZ film, and glass thermal resistances, respectively. Each thermal resistance depends on geometry (its thickness and area A) and thermal conductivity of the sample; then, expression (5) is given by [46–48]:

$$R_T = \frac{l_{YSZ}}{K_{YSZ}\,A} + \frac{l_{Glass}}{K_{Glass}\,A} \tag{6}$$

where l_{YSZ}, l_{Glass} and K_{YSZ}, K_{Glass} are the YSZ and glass thicknesses and thermal conductivities, respectively. The total thermal resistance also is

$$\frac{l_T}{K_T\,A} = \frac{l_{YSZ}}{K_{YSZ}\,A} + \frac{l_{Glass}}{K_{Glass}\,A} \tag{7}$$

http://dx.doi.org/10.5772/intechopen.81905

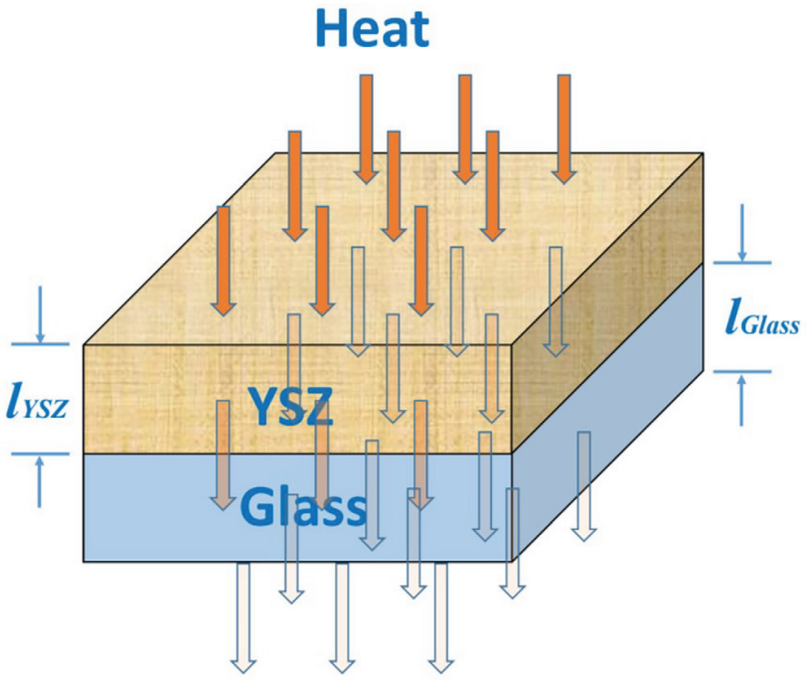

Figure 6. Schematic representation of the heat flow through the YSZ/glass double-layer sample.

Then, expression (7) can be written as

$$\frac{l_T}{K_T} = \frac{l_{YSZ}}{K_{YSZ}} + \frac{l_{Glass}}{K_{Glass}} \tag{8}$$

Here, l_T and K_T are the total thickness and the total thermal conductivity, respectively. And finally, from expression (8) the thermal conductivity in YSZ film can be determined as.

$$K_{YSZ} = \frac{l_{YSZ}}{[(l_T/K_T) - (l_{Glass}/K_{Glass})]} \tag{9}$$

Expression (9) requires knowing the thermal conductivity value of glass substrate, previously measured by using expression (4).

To determine the thermal conductivity of the 8YSZ coatings, these were deposited on glass substrates of known thermal conductivity values by using the procedure described by expression (9).

4. Effect of glancing angle deposition on the YSZ film properties

4.1. Film morphology

Cross-sectional images were carried out in a JEOL JSM-6490LV™ scanning electron microscopy. To show the effect of the oblique angle deposition on the microstructure of the thin films, a series of cross-sectional SEM images (**Figure 7**) were obtained by cleaving the samples

parallel to the grown "zigzag" structure. Due to YSZ non-conductive nature, a 5-nm gold layer was deposited to avoid charge accumulation during the measurements. A cross-sectional SEM image of an 8YSZ thin film grown with the conventional PVD geometry is shown as a reference in **Figure 7(a)**, where we can identify the parallel columnar structure normal to the surface, according to the Thornton diagram [12].

By applying an inclination of 45° between the vapor flow and the surface normal, the microstructure depicted in **Figure 7(b)** was obtained. The columnar structure is preserved but tilted toward the direction of the plasma plume with a column width similar to the reference sample. By turning the sample by 180° after half of the deposition, the column growth direction was also turned in-plane by 180° (**Figure 7(c)**). This "zigzag" structure is repeated without any degradation of the well-aligned columnar structure, as seen in **Figure 7(d)**. In **Figures 7(c)** and **7(d)**, we observe that the thicknesses of the column growth to the left are larger than to the right. This is because the thickness of the column growth depends greatly on the sample position in the sample holder (see **Figure 3a**).

However, when the number of repetitions increased to 10 (n = 10) and more (n = 30), then the "zigzag" structure appears within the columns, but the columns itself practically are not inclined, as we see in **Figure 8(a–d)**. In our case, the total coating thickness for all repetitions remains approximately constant (close to 3.5 μm), and for this reason, the time between repetitions is very short when n increases, for hence the columns do not reach to tilt as a whole.

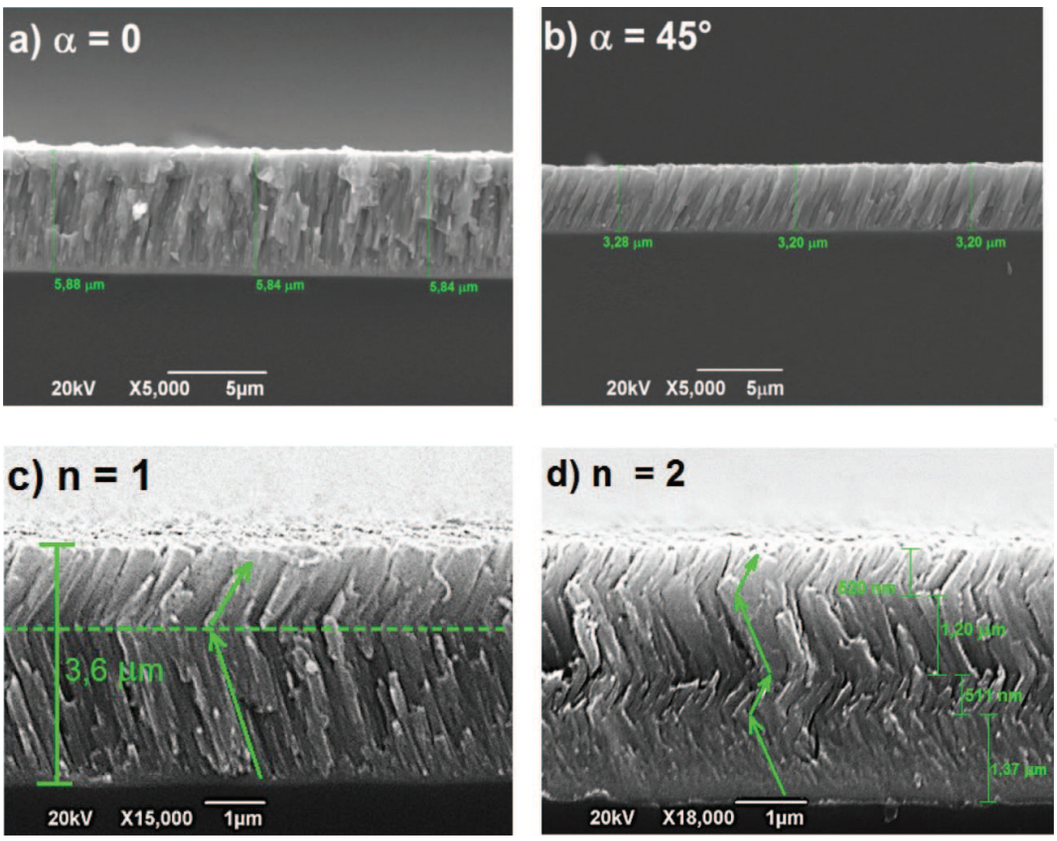

Figure 7. SEM cross-sectional views of YSZ thin films grown under (a) perpendicular incidence of the vapor flow to the substrate and (b)–(d) 45° of incidence [49].

http://dx.doi.org/10.5772/intechopen.81905

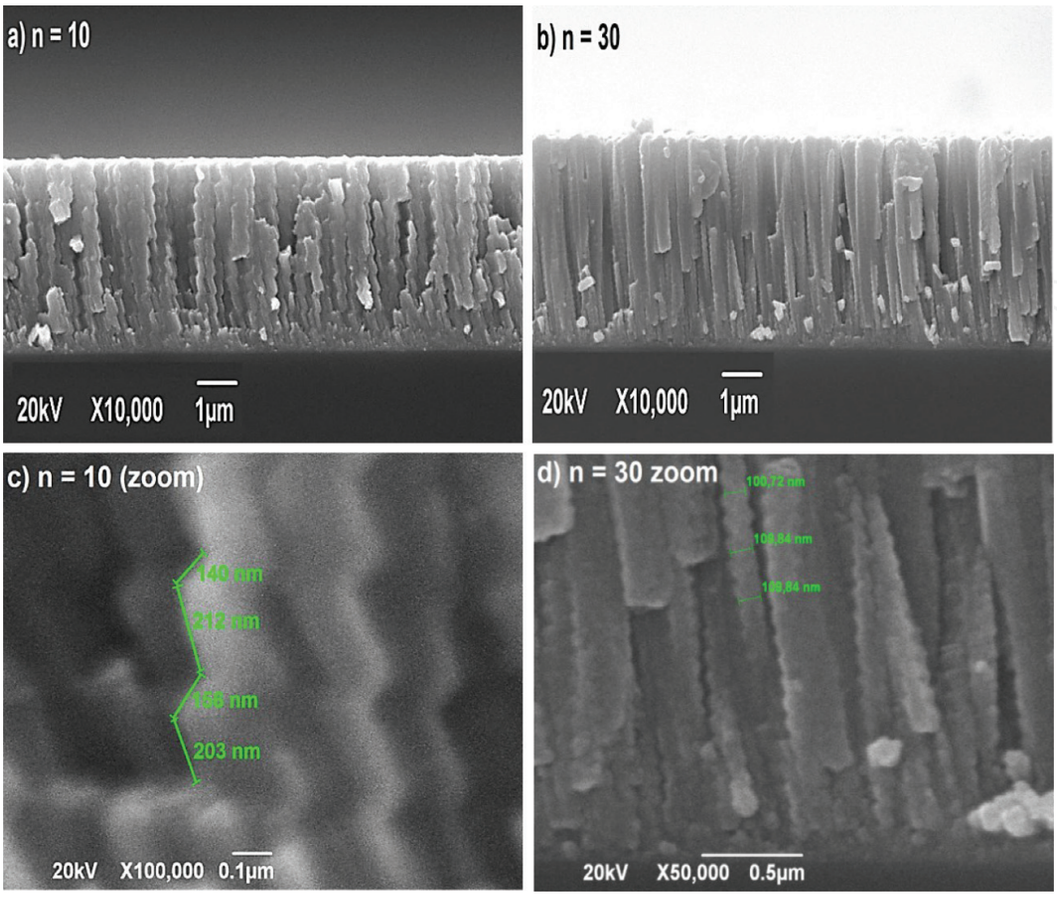

Figure 8. SEM cross-sectional views of YSZ thin films grown for (a) n = 10 and (b) n = 30; (c) and (d) provide details of the nanostructure within the columns [49].

4.2. Transmission electron microscopy analysis

In order to analyze the samples further, transmission electron microscopy (TEM) images recorded in cross-sectional lamellae of an 8YSZ thin film were carried out. Lamellae were prepared by focused ion beam (FIB) technique using a FEI Helios NanoLab 600i. TEM images were taken in a dedicated Hitachi HF-3300 (I2TEM-Toulouse) microscope operated at 300 kV. This microscope is equipped with a cold field emission gun and an image-aberration corrector (B-COR from CEOS), achieving a spatial resolution of 80 pm, in high-resolution TEM (HRTEM) mode [50].

Figure 9(a) displays an overview image for an 8YSZ multilayer with n = 10. We can see the substrate-multilayer interface and the zigzag microstructure. The total thickness of the multilayer is around 3.5 μm. In **Figure 9(b)**, we show a magnified area of the TEM image of **Figure 9(a)** around the kink (dashed lines) of the zigzag structure. Apparently, all columns continue to grow through the kink without any evidence of a discontinuous crystal structure as we can see in the high-resolution transmission electron microscope (HRTEM) micrographs (**Figure 9(c)** and **(d)**) corresponding to the zones labeled with red numbers 1 and 2 in **Figure 9(b)**. In addition, the contrast diffraction observed in such TEM images reveals that the oblique growth method induces the inclination of the crystallographic planes at $\alpha = 45°$ and $\alpha = -45°$ in the "thin" and

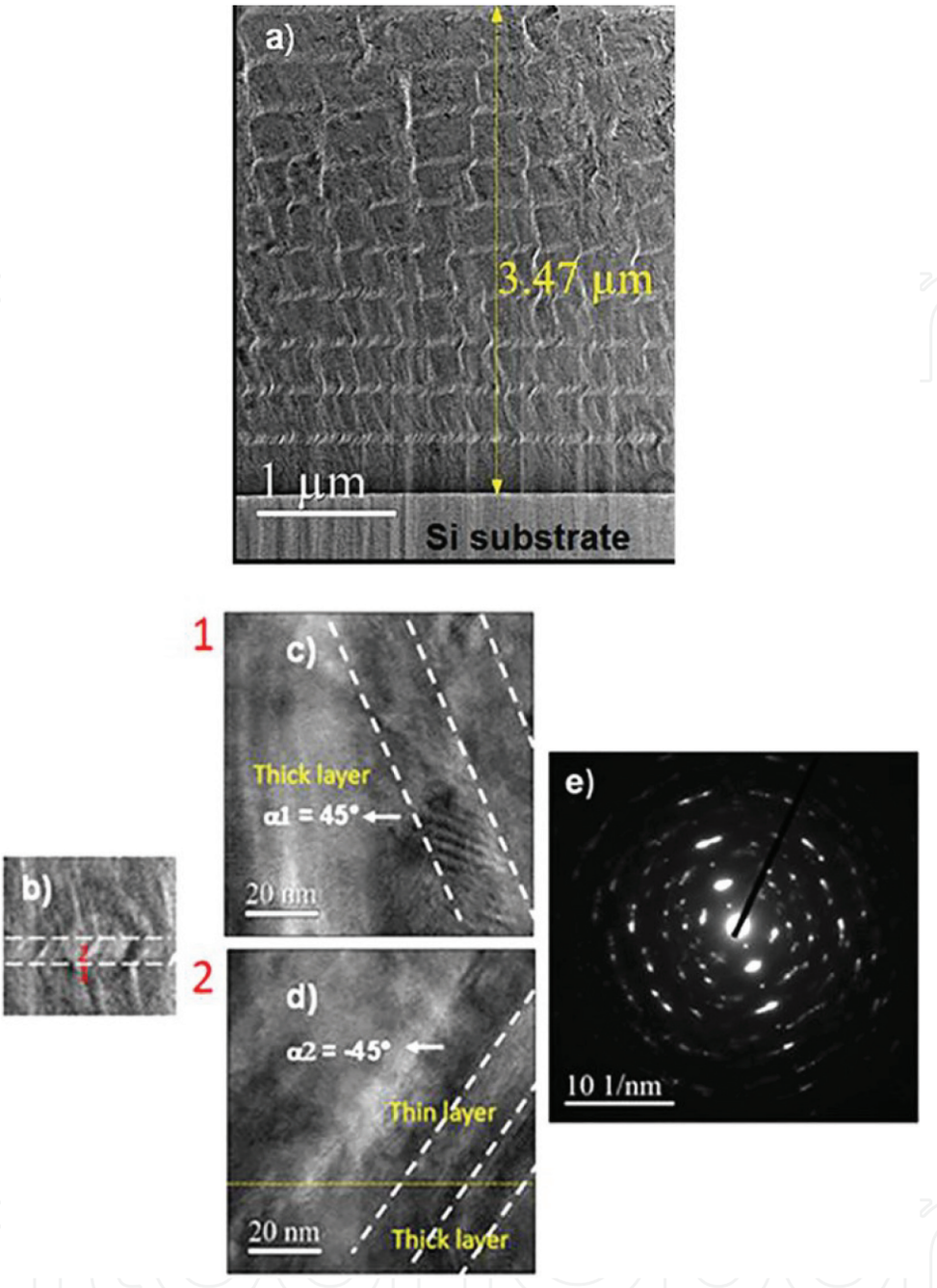

Figure 9. TEM micrographs for FIB lamella of a "zigzag"-structured YSZ thin film. (a) Low-magnification TEM image of the "zigzag" structure for n = 10. (b) Zoom around the dashed line in the low-magnification micrograph (a). HRTEM micrographs for the thickest region (c) labeled 1 in (b) and the thinnest (d) for the region labeled 2 in (b). Fast Fourier transform (FFT) pattern for thick (e) and thin (f) layers [49].

"thick" layers of the zigzag structure, respectively. Moreover, crystal diffraction patterns (**Figure 9 (e)** and **(f)**) obtained by applying a fast Fourier transform (FFT) on **Figures 9(c)** and **5(d)**, respectively, show that the microstructure of the YSZ films has a textured crystalline structure where some crystal planes are well defined in the HRTEM image. The angle that forms the twin can be determined from the angles that form the pyramidal faces to each other, in the images of TEM

micrographs. From the TEM image in **Figure 9b**, this angle was calculated as 75.94° for the +45° orientation.

4.3. X-ray diffraction microstructural analysis

For the microstructural analysis, X-ray diffraction (XRD) measurements were performed using a powder diffractometer Panalytical X'Pert PRO™ with a Cu Kα radiation source (λ = 1.54184 Å). **Figure 10a** and **11a** present the 8YSZ XRD patterns recorded in Bragg–Brentano geometry, for thin films deposited at a normal incident angle ($\alpha = 0°$) and at different repetition numbers of the "zigzag" structure (from n = 1 to n = 70), respectively. The XRD pattern of the 8YSZ film deposited at a normal incident angle ($\alpha = 0°$) shows a mixture of two phases: tetragonal zirconium yttrium oxide ($Zr_{0.94}Y_{0.06}O_{1.88}$) and monoclinic baddeleyite (ZrO_2) (JCPDF #01–089-9068 and #01–070-8739 cards, respectively). The preferred orientation on (002) plane of tetragonal phase is detected when n = 1, and its relative diffracted intensity increases gradually with n (**Figure 10a**). Moreover, (211) also shows a significantly preferred orientation of samples with n = 1, 2, and 10 "zigzag" arrays. The presence of silicon reflections of the substrate is very clear in the XRD pattern of the film growth at a normal incident angle and those with n = 1, 2, and 70. Samples with a great number of n (i.e., n = 30, 50, and 70) evolve toward a mono-axial preferential orientation on (002) plane; there is then a concomitant loss of orientation from pyramidal facets of {112} form. This latter behavior is a probable consequence of the increment of structural defects—disordered vacancies on Zr sites that affect

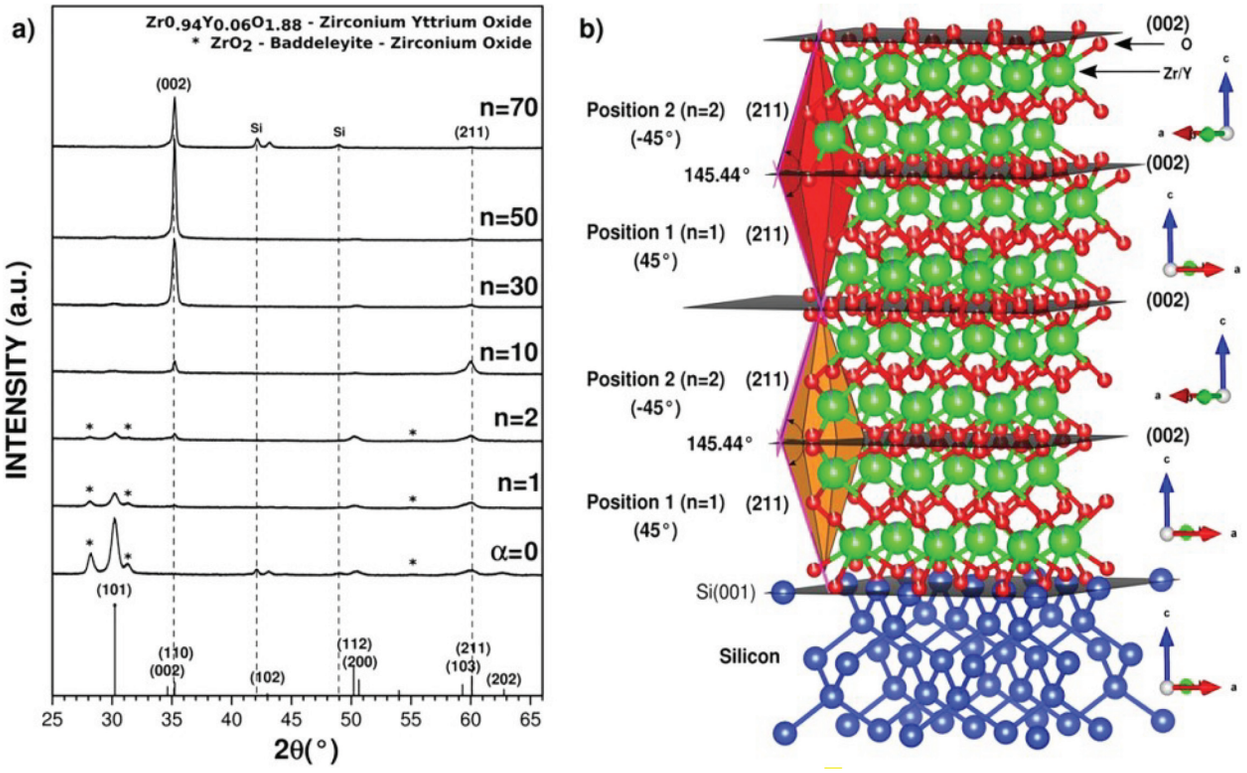

Figure 10. (a) XRD patterns of 8YSZ thin films deposited at a normal incident angle ($\alpha = 0$) and at different repetition numbers of the "zigzag" structure. (b) Schematic crystallographic simulation of the "zigzag" structure [49].

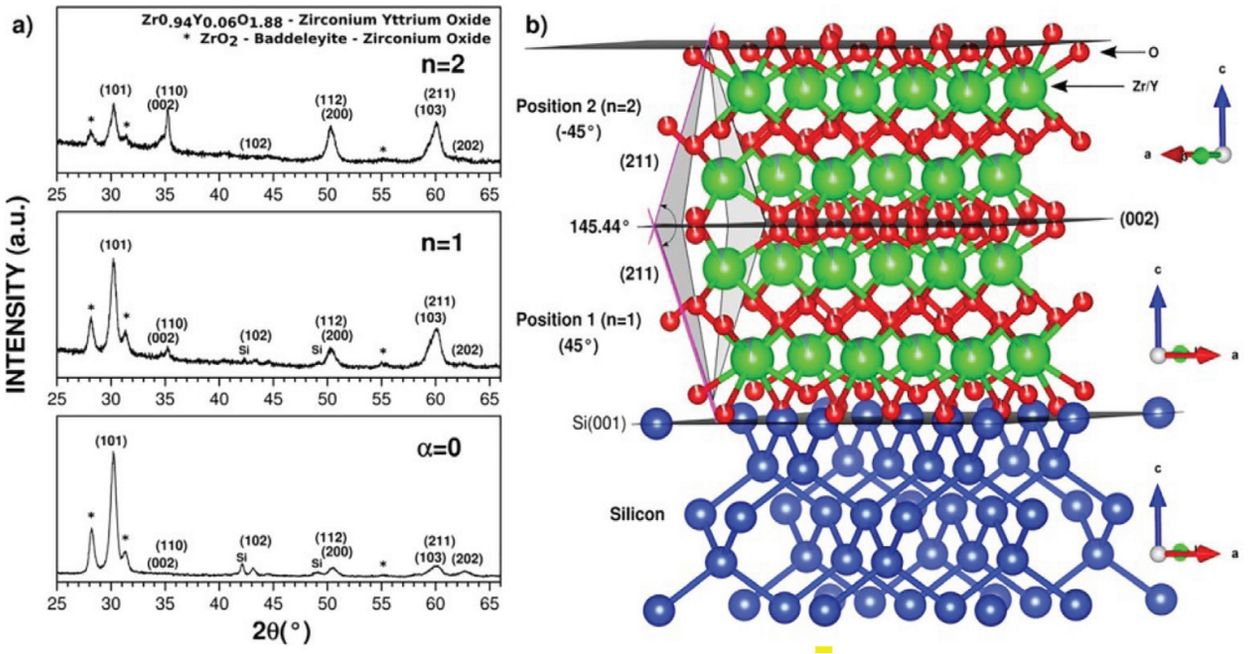

Figure 11. (a) XRD experimental data for films deposited at a normal incident angle (α = 0), n = 1 and n = 2 repetition numbers of the "zigzag" structure. (b) The schematic simulated crystallographic structure obtained from the experimental data [49].

directly the intensity of (211) reflection—as well as the profusion of both nano-porous and microstructural dislocations; thus, subsequent vertical columnar arrangement in the stacking arises, with the corresponding enhancement of the intensity on (002) diffraction peak.

Taking into account the predominance of the tetragonal structure and the multiaxial model of preferred orientations, as well as the "zigzag" features observed in SEM and TEM microphotographs for samples obtained from inclined experiments, a crystallographic simulation of the "zigzag" structure is proposed and graphically shown in **Figure 10b** and **11b**. The proposed microstructural model is based on the key role of a specific substrate tilt (e.g., $\pm\alpha$ = 45°) in promoting the growth of the tetragonal {211} bipyramidal facets on one side of the {001} planes, for example, (002) plane. The (002) is the twin plane in a contact twin where individual crystals are related by an inversion (i.e., 1). The growing direction is [001], and the surface of the twinned crystals is formed by {211} facets. In accordance with this scheme, when the tilt angle of the substrate is changed by 90° (from +45° to −45°), the {001} planes act as twin boundaries, with the subsequent growth of the pyramidal faces in a parallel but opposite direction. It is worth to note that a difference in length between both arms of twinned crystals is due to a different time of deposition.

The arrangement of the "zigzag" structures within the same level or, in other words, along with the direction [010], consists of a stacking of contiguous {211} facets. That is to say, the elbows are inter grooved along the direction of the bisector of the angle between two facets of the {211} form, for example, (−2–11) ^ (211) in **Figure 11b**, where complete bipyramidal morphologies are represented. The elbow angle results in 145.44° and the (002) ^ (211) is 72.72°. When the stacking

http://dx.doi.org/10.5772/intechopen.81905

of columnar twinned crystals is broken by profusion of defects as nano-porous, the relative intensity of (211) diminishes. This packing efficiency loss is clearly related to the occurrence of Si peaks in n = 70 XRD pattern. On the other hand, the enhancement of the intensity of twin plane (002) is a function of the number of tilt changes or "zigzag" structures. Accordingly, patterns show a dependence on the number of twin planes present in the film.

Thus, in our experiment, we obtain a polysynthetic twin. When α = 0°, neither preferred orientation nor silicon-dependent 8YSZ epitaxial growth has been observed.

4.4. Thermal conductivity behavior

To determine the thermal conductivity of the 8YSZ coatings, these were deposited on glass substrates of known thermal conductivity values by using the procedure described in paragraph 3. **Figure 12(a)** and **(b)** present the typical temperature evolution curves for the films deposited at a normal incident angle (α = 0) and at n = 10 number repetition of "zigzag" structure. In these curves, we see excellent agreement between the experimental data (black circles) and the fit to Eq. (3) (red curves). For the temperature evolution curves, three measurements for each sample were carried out, and the tolerance temperature of the measurements was 1 K.

From this fit, it is possible to obtain τ, which is directly related to the thermal conductivity (K) of the sample through Eq. (4) via procedure established by expression (9). Then, the effective thermal conductivity in the samples as film growth over glass substrates is obtained by using the double-layer method according to Eq. (9) [47, 48].

In **Figure 12(c)** summary of thermal conductivity behavior in all 8YSZ samples, for different values of α and n, is presented. For α = 0, the thermal conductivity (K) presents a value of 0.74 ± 0.05 W/mK, similar to that reported by Amaya et al. [19] of 0.57 ± 0.06 W/mK. Both values are for 8YSZ coatings grown via r.f. sputtering at equal deposition conditions with density, thermal diffusivity, and specific heat separately determined. As shown in **Figure 12(c)**, for 8YSZ coatings deposited with "zigzag" structure, the thermal conductivity (κ) drastically decreases in an order of magnitude when the number of bilayers n increases. However, for n = 70, the thermal conductivity starts to increase.

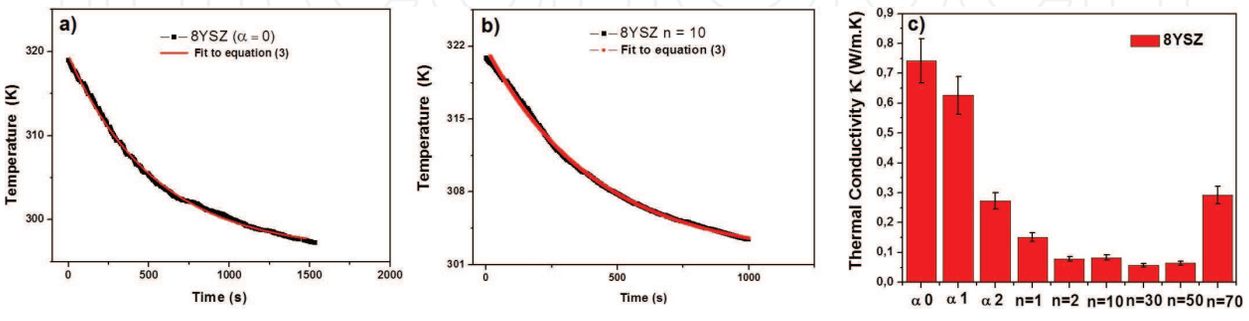

Figure 12. Typical temperature evolution curves for the films deposited at (a) normal incident angle (α = 0) and (b) n = 10 number repetition of "zigzag" structure. (c) Thermal conductivity evolution for α (0) (normal incident angle), α_1 (45°), α_2 (−45°), and n ranging from 1 to 70 repetitions of the "zigzag" structure [49].

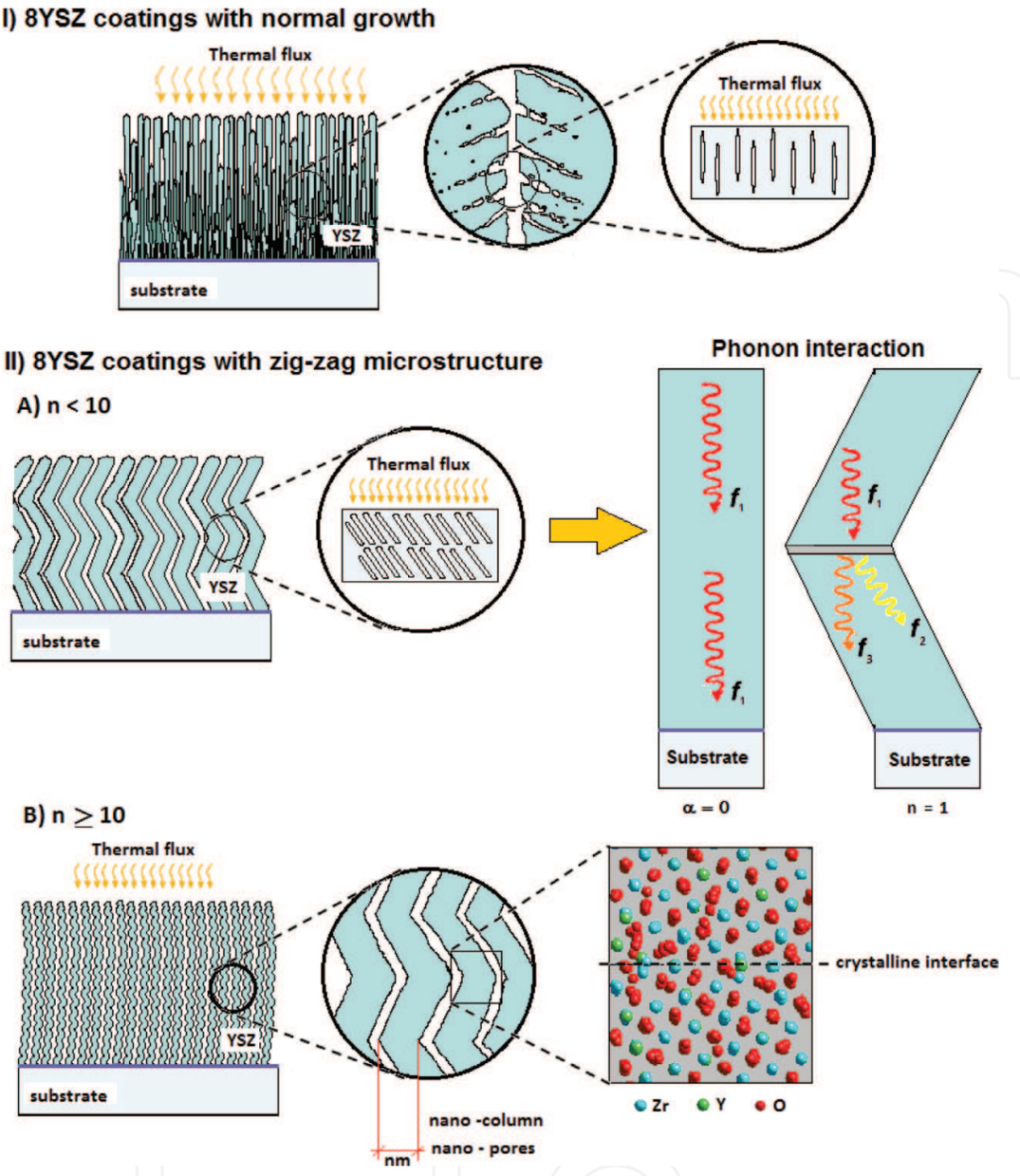

Figure 13. Schematic illustrations of (I) microstructure and porosity of PVD coatings and (II) influence of the "zigzag" microstructure on the YSZ coating thermal conductivity [49].

This thermal conductivity behavior of YSZ TBC is consistent with that obtained by Hass et al. [35], placing the substrate inclined with respect to the vapor flux to obtain a similar "zigzag" microstructure.

Heat thermal transport at nanometric scale is produced by phonons. Phonons have a wide variation in frequency and an even larger variation in their mean free paths (mfps). However, the bulk of the heat is often carried by phonons of a large wave vector, and they have mfps of 1–100 nm at room temperature.

Thereby, in many systems similar to those studied here, the scale of the phonon scattering centers has the same scale as the mfps of phonons, sometimes comparable to phonon wavelength. Due

http://dx.doi.org/10.5772/intechopen.81905

to this, either the interfaces or twist boundaries of the same material can play a critical role in nanoscale thermal transport [51, 52]. In this sense, we propose a phenomenological interpretation to explain the reduction in thermal conductivity when the value of (n) for the "zigzag" columns increases, with respect to the thermal conductivity of the coating deposited with a growth of columns normal to the substrate surface.

Figure 13-I shows the parallel thermal flux incidence with respect to the growth of columns for the 8YSZ coatings deposited with the normal direction of the incident flux of the species, with respect to the substrate surface. In contrast, **Figure 13-II(A)** at n < 10 samples indicates that when coatings are deposited under an oblique angle, a "zigzag" structure appears creating inclined crystallographic interfaces. Taking the column as an individual element, (α = 0), the heat flow is distributed in a longitudinal direction due to the growth direction that is normal to the substrate; therefore, the phonon scattering is due to the presence of the oxygen vacancies. When the oblique angle deposition takes place (n = 1), there is a change in the growth direction of the column, and as a result of this, an interface is generated, with which the heat carriers interact, scattering the heat flow into two components, a vertical component and a lateral component, due to the inclusion of the zigzag microstructure. This makes the mean free path of phonons to diminish due to the interaction of heat carriers with these interfaces, thus decreasing the thermal conductivity of the sample.

However, at n ≥ 10 (**Figure 13-II(B)**), the zigzag structure appears within the columns, which are practically not inclined but emerge the formation of nanopores between columns, and crystallographic interfaces contribute to greater phonon dispersion. Finally, increased thermal conductivity for n = 70 may be related to the fact that the total coating thickness for all repetitions remains approximately constant (close to 3.5 μm). For this reason, the time between repetitions is quite short, and the columns do not reach tilt as a whole, increasing the nanopore size; therefore, the mfp of phonons begins to increase again.

5. Conclusions

The oblique angle deposition is a powerful technique to modify the microstructure of PVD coatings deposited by sputtering in the micro- and nanometer scale, with high reproducibility and repeatability as the period (n) varied. For low values of repetition number (n = 10), the "zigzag" structure of 8YSZ coatings can be repeated without any degradation. However, when *n* increases from 10 to 70, the well-aligned columnar structure with "zigzag" microstructure has a columnar diameter refinement and the columns in the nanometer range growth perpendicular to the substrate surface, changing the orientation of porosity in the coatings. From the XRD and TEM analyses, it was established that twins are being produced to improve the thermal insulation properties. In fact, the thermal conductivity study allows to establish that the *k* value is strongly influenced by the "zigzag" microstructure of the PVD coatings, with a decrease of the thermal conductivity in an order of magnitude, when the columns change from normal growth orientation (α = 0) with respect to the substrate surface to a microstructure in a "zigzag" pattern with n = 50 repetitions, showing the potential of growing YSZ thin films in

glancing angle deposition, as an effective method to improve the thermal insulator property of this material.

Acknowledgements

This research was supported by funds for internal calls for projects at the Universidad del Valle 2013 (CI 7923) and by the Center of Excellence for Novel Materials (CENM) and ASTIN-SENA, Colombia. The authors would like to thank Dr. Pedro Prieto from the CENM and Dr. Luis Yate, Platform Manager of CIC biomaGUNE at Donostia-San Sebastián, Spain, for the AFM analysis.

Author details

Cesar Amaya[1,2], John Jairo Prıas-Barragan[3], Julio Cesar Caicedo[4], Jose Martin Yañez-Limon[5] and Gustavo Zambrano[1]*

*Address all correspondence to: gustavo.zambrano@correounivalle.edu.co

1 Department of Physics, Universidad del Valle, Cali, Colombia

2 Development of Materials and Products Research Group, CDT-ASTIN SENA, Cali, Colombia

3 Interdisciplinary Institute of Sciences and Electronic Instrumentation Technology Program, Universidad del Quindío, Armenia, Colombia

4 Tribology, Powder Metallurgy and Processing of Solid Recycled Research Group, Universidad del Valle, Cali, Colombia

5 Department of Materials Science and Engineering, Cinvestav-Unidad Querétaro, Querétaro, Mexico

References

[1] Meier SM, Gupta DK. Trans. ASME. The evolution of thermal barrier coatings in gas turbine engine applications. Journal of Engineering for Gas Turbines and Power. 1994;**116** (1):250-257

[2] Skinner SJ, Kilner JA. Oxygen ion conductors. Materials Today. 2003;**6**(3):30-37

[3] Fujikane M, Setoyama D, Nagao S, Nowak R, Yamanaka S. Nanoindentation examination of yttria-stabilized zirconia (YSZ) crystal. Journal of Alloys and Compounds. 2007;**431** (1–2):250-255

[4] Wortman DJ, Nagaraj BA, Duderstadt EC. Thermal barrier coatings for gas turbine use. Materials Science and Engineering. 1989;**A121**:443

[5] Gell M et al. Bond strength, bond stress and spallation mechanisms of thermal barrier coatings. Surface and Coating Technology. 1999;**53-60**:120-121

[6] Koosloos MFJ, van Liempd GG, Houben JM. Effect of local thermal shock load on plasma sprayed thermal barrier coatings. Surface Engineering. 1998;**14**(2):144

[7] Unal O, Mitchell TE, Heuer AH. Microstructures of Y_2O_3-Stabilized ZrO_2 Electron Beam-Physical Vapor Deposition Coatings on Ni-Base Superalloys. Journal of the American Ceramic Society. 1994;**77**(4):984-992

[8] Claves D, Galerie A. Kinetic and morphologic study of the pack-aluminization of a series of refractory alloys. Journal de Physique IV. 1993;**C9**:531

[9] Messier R, Giri AP, Roy RA. Revised structure zone model for thin film physical structure. Journal of Vacuum Science and Technology A. 1984;**2**:500

[10] Hultman L, Munz WD, Musil J, Kadlec S, Petrov I, Greene JE. Low-energy (∼100 eV) ion irradiation during growth of TiN deposited by reactive magnetron sputtering: Effects of ion flux on film microstructure. Journal of Vacuum Science & Technology, A: Vacuum, Surfaces, and Films. 1991;**9**:434

[11] Heiroth S, Lippert T, Wokaun A, Döbeli M, Rupp JLM, Scherrer B, et al. Yttria-stabilized zirconia thin films by pulsed laser deposition: Microstructural and compositional control. Journal of the European Ceramic Society. 2010;**30**(2):489-495

[12] Thornton JA. Influence of apparatus geometry and deposition conditions on the structure and topography of thick sputtered coatings. Journal of Vacuum Science and Technology. 1974;**11**:666

[13] Jones RL. Experiences in seeking stabilizers for zirconia having hot corrosion-resistance and high temperature tetragonal (t') stability (NRL/MR/6170–96–7841, Naval Research Laboratory; 1996

[14] Morrell P, Taylor R. Thermal diffusivity of thermal barrier coatings of ZrO_2 stabilized with Y_2O_3. High Temperatures - High Pressures. 1985;**17**:79

[15] Kyongjun A, Ravichandran KS, Semiatin SL. Microstructure, texture, and thermal conductivity of single-layer and multilayer thermal barrier coatings of Y_2O_3-stabilized ZrO_2 and Al_2O_3 made by physical vapor deposition. Journal of the American Ceramic Society. 1999;**82**(2):299

[16] Filla BJ. A steady-state high-temperature apparatus for measuring thermal conductivity of ceramics. The Review of Scientific Instruments. 1997;**68**(7):2822

[17] Portal R. Etude de la conductivite thermique de couches minces de ZrO_2-Y_2O_3 deposees par EB-PVD. Rapport de stage SNECMA; 1997

[18] Kabacoff LT. Thermally sprayed nano-structured thermal barrier coatings. NATO Workshop on Thermal Barrier Coatings, Aalborg, Denmark, AGARD-R-823; 1998, paper 12

[19] Amaya C, Caicedo JC, Yáñez-Limón JM, Vargas RA, Zambrano G, Gomez ME, et al. A non-destructive method for determination of thermal conductivity of YSZ coatings deposited on Si substrates. Materials Chemistry and Physics. 2012;**136**:917

[20] Klemens PG, Gell M. Thermal conductivity of thermal barrier coatings. Materials Science and Engineering A. 1998;**245**:143-149

[21] Soyez G, Eastman JA, Thompson LJ, Bai GR, Baldo PM. Grain-size-dependent thermal conductivity of nanocrystalline yttria-stabilized zirconia films grown by metal-organic chemical vapor deposition. Applied Physics Letters. 2000;**77**(8):1155-1157

[22] Lee S-M, Matamis G, Cahill DG. Thin-film materials and minimum thermal conductivity. Microscale Thermophysical Engineering. 1998;**2**:31-36

[23] An K, Ravichandran KS, Dutton RE, Semiatin SL. Microstructure, texture, and thermal conductivity of single-layer and multilayer thermal barrier coatings of Y_2O_3-stabilized ZrO_2 and Al_2O_3 made by physical vapor deposition. Journal of the American Ceramic Society. 1999;**82**(2):399-406

[24] Nicholls JR, Lawson KJ, Johnstone A, Rickerby DS. Low thermal conductivity EB-PVD thermal barrier coatings. Materials Science Forum. 2001;**369**(372):595

[25] Wolfe DE, Singh J, Miller RA, Eldridge JI, Zhu DM. Tailored microstructure of EB-PVD 8YSZ thermal barrier coatings with low thermal conductivity and high thermal reflectivity for turbine applications. Surface and Coating Technology. 2005;**190**:132-149

[26] Knorr TG, Hoffman RW. Dependence of geometric magnetic anisotropy in thin iron films. Physics Review. 1959;**113**:1039

[27] Robbie K, Sit JC, Brett MJ. Advanced techniques for glancing angle deposition. Journal of Vacuum Science and Technology B. 1998;**16**:1115

[28] Malac M, Egerton R. Observations of the microscopic growth mechanism of pillars and helices formed by glancing-angle thin-film deposition. Journal of Vacuum Science & Technology, A: Vacuum, Surfaces, and Films. 2001;**19**:158

[29] Lakhtakia A, Messier R. Sculptured thin films: Nanoengineered morphology and optics. In: Society of Photo–Optical. Bellingham, WA, USA: SPIE Press; 2005

[30] Takadoum J, Lintymer J, Gavoille J, Martin N. Chromium multilayered thin films with orientated microstructure. Journal de Physique IV France. 2005;**123**:137

[31] Lintymer J, Gavoille J, Martin N, Takadoum J. Glancing angle deposition to modify microstructure and properties of sputter deposited chromium thin films. Surface and Coating Technology. 2003;**174, 175**:316

[32] Stender D, Schäuble N, Weidenkaff A, Montagne A, Ghisleni R, Michler J, et al. Dense zig-zag microstructures in YSZ thin films by pulsed laser deposition. APL Materials. 2015; **3**(1):016104

[33] Motohiro T, Taga Y. Thin film retardation plate by oblique deposition. Applied Optics. 1989;**28**:2466

[34] Robbie K, Brett MJ, Lakhtakia A. Chiral sculptured thin films. Nature. 1996;**384**:616

[35] Hass DD, Slifka AJ, Wadley HNG. Low thermal conductivity vapor deposited zirconia microstructures. Acta Materialia. 2001;**49**:973

[36] van Kranenburg H, Lodder JC. Tailoring growth and local composition by oblique-incidence deposition: a review and new experimental data. Materials Science & Engineering R: Reports. 1994;**11**:293

[37] Zambrano Romero GA, Gómez de Prieto ME, Prieto Pulido PA, Caicedo Angulo JC y Amaya Hoyos CA. Dispositivo para deposito en ángulo oblicuo de materiales a escalas nano y micrométricas mediante técnicas PVD. Co-patent 14-185631; 2016

[38] Baba T, Ono A. Improvement of the laser flash method to reduce uncertainty in thermal diffusivity measurements. Measurement Science and Technology. 2001;**12**:2046-2057

[39] Mayen Mondragon R, Yàñez-Limòn JM. Study of blue phases transition kinetics by thermal lens spectroscopy in cholesteryl nonanoate. The Review of Scientific Instruments. 2006;**77**:044903–1-044903–7

[40] Alvarado-Gil JJ, Zelaya-Angel O, Sanchez-Sinencio F, Yáñez Limón JM, Vargas H, Figueroa JCC, et al. Photoacoustic monitoring of processing conditions in cooked tortillas: Measurements of thermal diffusivity. Journal of Food Science. 1995;**60**:438-442

[41] Rosencwaig A, Gersho A. Theory of the photoacoustic effect of solids. Journal of Applied Physcis. 1976;**47**:64-69

[42] Bento AC, Dias DT, Olenka L, Medina AN, Baesso ML. On the application of the photoacoustic methods for the determination of thermo-optical properties of polymers. Brazilian Journal of Physics. 2002;**32**:483-494

[43] Mandelis A, Zver MM. Theory of photopyroelectric spectroscopy of solids. Journal of Applied Physics. 1985;**57**:4421-4430

[44] Cahill DG. Thermal conductivity measurement from 30 to 750 K: The 3 omega method. Review of Scientific Instruments. 1990;**61**(2):802-808

[45] Schmidt AJ, Cheaito R, Chiesa M. A frequency-domain thermoreflectance method for the characterization of thermal properties. Review of Scientific Instruments. 2009;**80**:094901–6

[46] Prías-Barragán JJ, Muñoz-Gómez AP, Ariza-Calderón H. System for Measuring Thermal Conductivity in Multiple Solid Samples. Co-patent 2012-9821

[47] González de la Cruz G, Gurevich YG, Logvinov GN, Muñoz Aguirre N. Superficies Vacío. 2000;**10**:40

[48] Mansanares AM, Bento AC, Vargas H, Leite NF. Physical Review B. 1995;**42**:4477

[49] Amaya C, Prías-Barragán JJ, Aperador W, Hernández-Landaverde MA, Ramírez-Cardona M, Caicedo JC, et al. Thermal conductivity of yttria-stabilized zirconia thin films with a zigzag microstructure. Journal of Applied Physics. 2017;**121**:245110

[50] Snoeck E, Houdellier F, Taniguch Y, Masseboeuf A, Gatel C, Nicolai J, et al. Off-axial aberration correction using a B-COR for lorentz and HREM modes. Microscopy and Microanalysis. 2014;**20**(S3):932

[51] Cahill DG, Ford WK, Goodson KE, Mahan GD, Majumdar A, Maris HJ, et al. Nanoscale thermal transport. Journal of Applied Physics. 2003;**93**:793

[52] Cahill DG, Braun PV, Chen G, Clarke DR, Fan S, Goodson KE, et al. Nanoscale thermal transport. II. 2003–2012. Applied Physics Reviews. 2014;**1**:011305